Med Biol Eng Comput (2013) 51:757–768
DOI 10.1007/s11517-013-1042-9

ORIGINAL ARTICLE

Estimation of impulse response between electromyogram signals for use in conduction delay distribution estimation

Tahsin Hassan · Kyle C. D. McIntosh · David A. Gabriel · Edward A. Clancy

Received: 22 May 2012 / Accepted: 22 January 2013 / Published online: 6 February 2013

Abstract The time delay between two surface electromyograms (EMGs) acquired along the conduction path is used to estimate *mean* action potential conduction velocity. Modeling the linear impulse response between "upstream" and "downstream" EMG signals permits an estimate of the *distribution* of velocities, providing more information. In this work, we analyzed EMG from bipolar electrodes placed on the tibialis anterior of 36 subjects, using an inter-electrode distance of 10 mm. Regularized least squares was used to fit the coefficients of a finite impulse response model. We trained the model on one recording, then tested on two others. The optimum correlation between the model-predicted and actual EMG averaged 0.70. We also compared estimation of the *mean* conduction delay from the peak time of the impulse response to the "gold standard" peak time of the cross-correlation between the upstream and downstream EMG signals. Optimal models differed from the gold standard by 0.02 ms, on average. Model performance was influenced by the regularization parameters. The impulse responses, however, incorrectly contained substantive power at very low time delays, causing delay distribution estimates to exhibit high probabilities at very short conduction delays. Unrealistic distribution estimates resulted. Larger inter-electrode spacing may be required to alleviate this limitation.

Keywords Electromyography · Conduction velocity · Conduction delay · Conduction delay distribution

T. Hassan · E. A. Clancy (✉)
Department of Electrical and Computer Engineering, Worcester Polytechnic Institute, Worcester, MA, USA
e-mail: ted@wpi.edu

T. Hassan
e-mail: thassan@wpi.edu

K. C. D. McIntosh · D. A. Gabriel
Faculty of Applied Health Sciences, Brock University, St. Catharines, ON, Canada
e-mail: km03ki@badger.ac.brocku.ca

D. A. Gabriel
e-mail: dgabriel@brocku.ca

1 Introduction

Electromyogram (EMG) conduction velocity (CV) refers to the speed of action potential propagation along the muscle fiber. Abnormal CV may indicate myopathic and neurologic disorders [1, 2, 31, 33] and CV slowing is associated with localized muscle fatigue and EMG spectral compression [3, 4, 24, 28, 32]. *Mean* CV is typically estimated by recording two interference-pattern surface EMG signals along the conduction path, then dividing the path length by the propagation delay (see [7] for a review). Both electrode recordings are acquired on one side of the innervation zone, with action potentials propagating first past the so-called "upstream" electrodes and thereafter past the "downstream" electrodes. The estimated delay averages the contributions from individual motor units (MUs) within the pick-up area of the electrodes, weighted by each MU amplitude. Methods for estimating mean propagation delay/conduction velocity from the EMG of two recording sites include the use of: spectral dips [9, 18], the delay between reference points in detected waveforms [15, 19, 20, 27], phase differences [17], maximum likelihood estimation [11, 13, 27] and cross-correlation [3, 24, 32].

Recorded signal components arriving simultaneously at both EMG sites—including power-line interference and nonpropagating EMG (e.g., end of fiber potentials)—bias the estimated delay towards shorter values (and, therefore, bias the conduction velocity towards higher values).

Double-difference electrodes have been used to reject these common signal components [3, 12, 23, 27]. Complex or optimized spatial and/or temporal filters may further reduce this error [6, 23, 27]. Multiple channel linear [10–12, 23] and two-dimensional [8, 13, 14, 31, 33] recording arrays have been used to track individual MU action potentials.

The classic two-site methods assume that all MUs are oriented along the line between the two electrodes and that *mean* CV is an appropriate measure. However, the underlying muscle fibers are not exactly parallel and each MU has a distinct conduction velocity. Thus, it is more informative to extract an estimate of the *distribution* of conduction delays/velocities. Based on the original work of Williams [30] on nerve bundles, Hunter et al. [17] related the distribution of conduction delays between two EMG sites to the absolute value of the impulse response between the upstream and downstream locations. This model assumes that the EMG signal due to individual MUs sum to produce the recorded interference pattern, the action potential shape of each MU is identical and each MU action potential arrives at the downstream electrode site after a pure (but distinct) time delay. The impulse response was estimated by solving a matrix equation relating the upstream–downstream EMG cross-correlation function to the upstream auto-correlation function and the impulse response (see the "indirect" estimate method described below). Their method was evaluated on one recording with a 15 mm inter-electrode distance. Davies and Parker [5] modeled multiple MU action potentials (with distinct conduction velocities) and fashioned an estimate of conduction velocity distribution also using auto- and cross-spectra. Their method was evaluated on one recording, using a 20 mm inter-electrode distance.

In this report, we further investigate estimation of the impulse response between a pair of conventional bipolar EMG electrodes separated by 10 mm as an approach to estimate propagation delay distribution. We introduce a more direct method to estimate the impulse response via a finite impulse response (FIR) model, comparing results to the method of Hunter et al. [17]. Our direct method estimates the impulse response via linear least squares. We therefore investigated two methods to regularize the resulting impulse response—the singular-value-decomposition-based pseudo-inverse approach [25] and an approach based on post hoc low-pass filtering of the FIR sequence. Performance was evaluated on EMG recordings from the tibialis anterior muscle of 36 subjects.

2 Methods

2.1 Experimental methods

A 36-subject (19 males, 17 females; aged 23.7 ± 3.0 years) subset of experimental data acquired for a prior study was reanalyzed. The original study [21, 22] was approved by the Brock University Research Ethics Board, with written informed consent secured from each subject. Data reanalysis was approved by the WPI IRB. Subjects had to be right leg dominant with a body mass index under 25.

Subjects lay supine while a constant-current source (150 mA, 1 ms duration square-wave pulse, rate of 10 pps) was used to find the motor point. The lower leg was shaved, abraded and cleansed with alcohol. A bar electrode was applied using two-sided tape and electrolyte gel. Recording electrodes on the bar consisted of four stainless-steel tubular surfaces, each 1 mm in diameter and 10 mm long, with an inter-electrode distance of 5 mm. The electrodes were configured to yield three bipolar signals from adjacent electrodes, of which the first and third (inter-electrode distance of 10 mm) were primarily utilized. The ground electrode was located on the lateral malleolus. For each experimental session, initial placement was in line with the muscle fibers, between the motor point and the distal tibialis anterior tendon. (This line was marked with indelible ink on the first day.) Electrically evoked potentials were then elicited and the electrode orientation manipulated until electrode placement/orientation maximized action potential shape similarity and delay between EMG channels [13]. Once the electrodes were secured, impedance was assessed to ensure that it was lower than 10 kΩ. If not, additional skin preparation was conducted until this criterion was met.

Subjects sat in a testing chair designed to isolate isometric ankle dorsiflexion. The chair was adjusted so that the hip and knee joints were at 90°, and the ankle joint was at 110°. Dorsiflexion forces were applied perpendicular to a load cell (JR3 Inc., Woodland, CA, USA) through an adjustable mount. A padded metal bar secured the top of the foot at the fifth metatarsal. Belts stabilized the subject within the chair. Subjects then performed three, 5-s duration, maximal voluntary contractions (MVCs) of the dorsiflexors, with a 3-min rest interval. After 5 min rest, 30 % MVC trials were conducted. Each 30 % MVC contraction lasted 5 s, including the force ramp-up period, isometric contraction (2–4 s duration) and the ramp-down period. The entire protocol was repeated a second day. Only the isometric contraction periods of the 30 % MVC trials were utilized in this study; in particular, one 30 % MVC from the first day (trial 1) and two from the second day (trials 2 and 3). Using data from both days increased the amount of available data for analysis, presumably increasing statistical power. The EMG signals were band-pass filtered between 10 and 1,000 Hz and amplified (Grass P511, Astro-Med Inc., West Warwick, RI, USA). The EMG and load cell force were sampled with 16-bit resolution at 5,000 Hz [21, 22].

2.2 Analysis models

2.2.1 EMG signal model

A simple, phenomenological model of EMG signal propagation between two sites along the conduction path is shown in Fig. 1, modified from Rababy et al. [26] via the addition of a second noise source (to balance the noises represented at each EMG site). Variable $x_1[n]$ is the noise-free "upstream" signal at sample n and $x_2[n]$ the noise-free "downstream" signal, neither of which is measurable. The finite-duration, linear, time-invariant filter $h[n]$ gives the impulse response between these two signals. Recorded signals $m_1[n]$ and $m_2[n]$ are corrupted by mutually independent additive noise sources $r_1[n]$ and $r_2[n]$, respectively.

From the model, the noise-free upstream and downstream EMG signals are related via convolution as:

$$x_2[n] = \sum_{i=-p_1}^{p_2} h[i] \cdot x_1[n-i], \tag{1}$$

where the positive-valued integers p_1 and p_2 specify the range of the finite impulse response (in samples). Parameter p_1 specifies "system anticipation" and p_2 specifies "system memory", both of which are necessary to capture the system dynamics, even when modeling pure time delays [16]. Accounting for the additive noise sources allows this equation to be written in terms of the measurable EMG signals as:

$$m_2[n] - r_2[n] = \sum_{i=-p_1}^{p_2} h[i] \cdot \{m_1[n-i] - r_1[n-i]\},$$

or

$$m_2[n] = \sum_{i=-p_1}^{p_2} h[i] \cdot m_1[n-i] + e[n], \tag{2}$$

where $e[n] = r_2[n] - \sum_{i=-p_1}^{p_2} h[i] \cdot r_1[n-i]$ represents an error term.

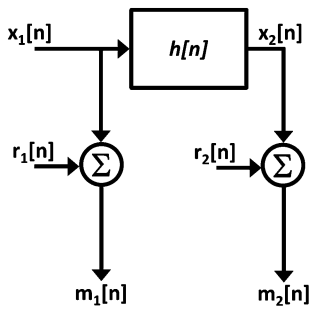

Fig. 1 Action potential propagation model. Signal $x_1[n]$ is the noise-free "upstream" signal, $x_2[n]$ is the noise-free "downstream" signal, $h[n]$ gives the impulse response between them. Recorded signals $m_1[n]$ and $m_2[n]$ are corrupted by mutually uncorrelated additive noise sources $r_1[n]$ and $r_2[n]$, respectively

2.2.2 "Direct" estimate of the impulse response

The finite impulse response $h[n]$ consists of $p_1 + p_2 + 1$ unknown sequence values. Let the measured EMG signals $m_1[n]$ and $m_2[n]$ be known over N samples, with $N \gg p_1 + p_2 + 1$. Linear least squares can be used to optimally estimate the $h[n]$ sequence [25]. Note that $p_1 + p_2$ additional samples from $m_1[n]$ and $m_2[n]$ (i.e., outside of the original range of N samples) are actually utilized in order to satisfy the future and past lags specified in the sum in Eq. (2).

In practice, solution to this least squares problem is ill-conditioned. As will be shown in Sect. 3, the unconditioned solution produces an impulse response sequence with excessive high-frequency noise. Thus, two methods were used to regularize the solution. First, we investigated the singular-value-decomposition-based least squares pseudo-inverse approach, in which certain linear combinations of the training data—those that likely provide little information, but contain considerable noise—are omitted from the training solution [25]. The tolerance for omission was based on the ratio of each singular value to the maximum singular value. Note that this tolerance definition differs from that found in the MATLAB *pinv* command. Second, we low-pass filtered the impulse response after the least squares fit. A fourth-order Butterworth filter was designed, then applied in the forward and reverse time directions, to achieve zero phase. This process leaves both a head and tail startup transient. These transients were omitted by extracting a sub-segment of the filtered impulse response, over a range specified by $p_{1\_Extract}$ and $p_{2\_Extract}$, respectively. The overall filter impulse response range (specified by p_1 and p_2) was large enough so that the discarded samples occurred outside the plausible range of conduction delays.

2.2.3 "Indirect" estimate of the impulse response

An indirect method for estimating the finite impulse response based on Eq. (2) has previously been described [17]. Briefly, if we substitute $n + k$ for n, multiply both sides of the equation by $m_1[n]$ and then average over N sample values:

$$\frac{1}{N}\sum_{n=0}^{N-1} m_1[n] \cdot m_2[n+k] = \sum_{i=-p_1}^{p_2} h[i] \cdot \frac{1}{N}\sum_{n=0}^{N-1} m_1[n] \cdot m_1[n+k-i] + e'[k], \tag{3}$$

where $e'[k] = \frac{1}{N}\sum_{n=0}^{N-1} m_1[n] \cdot e[n+k]$ is an error term. The left side of Eq. (3) is the biased cross-correlation estimate, $R_{m_1 m_2}[k]$. Similarly, the right side contains the biased auto-correlation, $R_{m_1 m_1}[k-i]$, giving:

$$R_{m_1 m_2}[k] = \sum_{i=-p_1}^{p_2} h[i] \cdot R_{m_1 m_1}[k-i] + e'[k]. \quad (4)$$

The finite impulse response sequence in Eq. (4) can now be solved via linear least squares over the range of available correlation values. With this indirect approach, we also examined the singular-value-decomposition-based pseudo-inverse approach and post hoc low-pass filtering, utilizing the same tolerance values/cutoff frequencies as with the direct approach.

2.3 Methods of analysis

Our goal was to evaluate different methods for estimating the finite impulse response when neither the true impulse response nor the true distribution of delays is known. Therefore, we used several indirect measures of performance. All analysis was performed in MATLAB (MathWorks, Natick, MA, USA). Statistical comparisons utilized paired *t* tests (with Bonferroni adjustment) and ANOVAs, as further detailed within Sect. 3.

First, we visually evaluated the impulse response produced by the direct method, as well as the magnitude of its discrete Fourier transform (DFT), on a subset of the 36 subjects. Since the finite range of the impulse response affects the determined response, we evaluated seven different duration parameter sets, denoted scenarios in Table 1, selected after some initial heuristic evaluation. When using the pseudo-inverse approach, the tolerance values investigated were: 0.9, 0.8, 0.7, 0.6, 0.5, 0.4, 0.3, 0.2, 0.1, 10^{-2}, 10^{-3}, 10^{-4}, 10^{-5} and 10^{-6}. Large tolerance values denote that many singular values were discarded from the inverse. When using the post hoc filtering approach, the low-pass filter cutoff frequencies were: 25, 50, 75, 100, 125, 150, 175, 200, 225, 250, 275, 300, 325, 350, 400, 450, 500, 600, 850 and 1,000 Hz. This least squares inverse was computed using the pseudo-inverse with default MATLAB tolerance (a very small tolerance value, related to the numerical precision).

Table 1 Scenarios (parameter combinations) used to evaluate impulse response performance, in milliseconds (ms)

Scenario	p_1 (ms)	$p_{1\_Extract}$ (ms)	p_2 (ms)	$p_{2\_Extract}$ (ms)
1	5	4	10	5
2	20	9	20	5
3	16	9	20	5
4	12	5.6	10	5
5	8	4	12	5
6	20	10	20	5
7	0	0	5	5

Second, we evaluated the representativeness of the model shown in Fig. 1 by training a model (i.e., calibrating an impulse response) to the first 30 % MVC recording from each subject (trial 1), then testing that model on trials 2 and 3. Each test passed the upstream EMG data through the impulse response and then compared that filtered output to the measured downstream EMG. The correlation coefficient was our metric of goodness of fit, since we did not want changes in signal gains to influence the metric (nonetheless, similar results were found when evaluating mean squared error). Results from the two test trials per subject were averaged. The tolerances and low-pass cutoff frequencies listed above were investigated, for both the direct and indirect model solution techniques.

Third, an appropriately modeled impulse response typically exhibits a single dominant peak, whose time location represents the mean conduction delay [17]. However, if only the mean conduction delay is desired, it is more common to use the time location of the peak of the cross-correlation function between the upstream and downstream signals [3, 24, 32]. Thus, we compared the mean conduction delay determined by the "gold standard" cross-correlation method to that determined from the dominant peak of the impulse response. For the cross-correlation method, the EMG signals were upsampled by a factor of 10 (to a rate of 50 kHz). To do so, the original data samples were interpolated by inserting nine zero values between each sample, followed by low-pass filtering (MATLAB *interp* command). Impulse responses were similarly upsampled prior to locating their peak. Upsampling provided a timing delay resolution of 20 μs. The absolute error between the delay estimated by the cross-correlation and impulse response methods was determined for each of the two 30 % MVC test trials (trials 2 and 3), and then averaged. For the impulse response method, the impulse response was estimated from trial 1. The same tolerances and low-pass cutoff frequencies as listed above were investigated, for both the direct and indirect model solution techniques.

3 Results

Figure 2 shows data from an example 30 % MVC recording and the corresponding EMG power spectrum. Most of the EMG power occurred below 300 Hz, with very little power above 400 Hz. Conduction delay analysis was only performed on stable portions of each 30 % MVC recording, identified via manual selection. The available durations ranged from 2.56 to 4.44 s, with a mean ± standard deviation (SD) duration of 3.45 ± 0.44 s.

Figures 3 (pseudo-inverse tolerance approach) and 4 (post hoc low-pass filtering approach) illustrate the range of impulse responses encountered during the visual

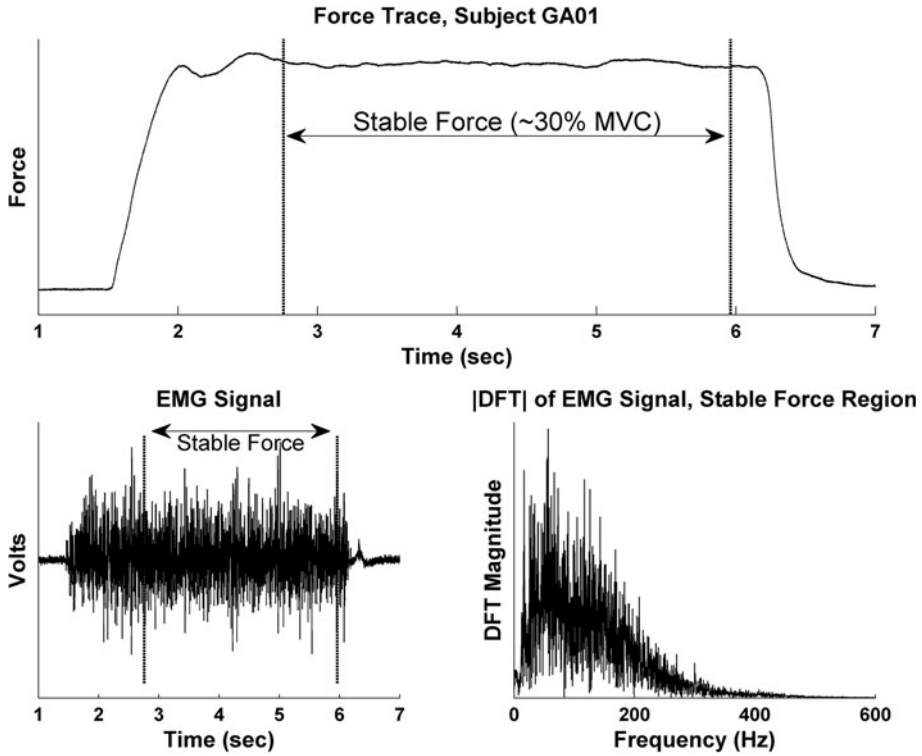

Fig. 2 Sample force recording (*top*) and corresponding EMG signal (*lower left*). *Bottom right* shows DFT magnitude of the EMG signal. Subject produced a 30 % MVC during the time region marked "Stable Force"

evaluations of the direct solution method. Several characteristics are seen. First, the right-most column of Fig. 3 uses a pseudo-inverse tolerance that is so small (10^{-25}) that this result approximates use of a standard matrix inverse in the least squares procedure. The impulse response exhibits significant high-frequency noise, well outside the bandwidth of the EMG signals. From a frequency domain perspective, the impulse response can be thought of as the inverse DFT of the transfer function between the upstream and downstream EMG signals. The transfer function is the DFT of the downstream signal divided by the DFT of the upstream signal. At high frequencies, both EMG signals contain little power. Thus, division at the high frequencies—division of two very small magnitudes—produces erratic profiles. Second, the middle column of Fig. 3 shows more reasonable time and frequency domain results. Here, the pseudo-inverse tolerance of 0.2 has essentially smoothed the impulse response. The singular vectors associated with the discarded singular values characteristically contain higher frequency components. Third, if the pseudo-inverse tolerance is increased too much then excessive smoothing of the impulse response results (left column of Fig. 3, tolerance of 0.9). In this case, too few singular vectors were retained, thereby failing to capture enough system dynamics. Fourth, Fig. 4 shows that qualitatively similar trends occur when post hoc low-pass filtering is applied. Too little low-pass filtering produces excessive high-frequency gains. When the impulse response is limited to a frequency band similar to that of the original signals (cutoff frequency of 250 Hz), a visually appropriate impulse response/transfer function is produced. When the low-pass filter is overly restrictive, an over-smoothed impulse response is produced. Startup errors are visible in each impulse response outside of the $p_{1\_Extract}$ to $p_{2\_Extract}$ range. Fifth, visual evaluation (not shown) of results in which both the pseudo-inverse tolerance approach and post hoc low-pass filtering were applied in cascade suggested no additional dimension of response variation.

The above results show that varying the tolerance value/low-pass cutoff frequency provides a trade-off between under-smoothing and over-smoothing the impulse response. To quantify this trade-off, the model was evaluated by training the model to one 30 % MVC trial, then testing that model on the two remaining 30 % MVC trials. Figure 5 shows the average cross-correlation results between the actual and model-estimated "downstream" EMG signals. In general, as the tolerance value was decreased or low-pass filter cutoff frequency increased, there was an initial stage of transient performance, followed by a plateau of stable performance. For the best scenarios—numbers 5 and 6 (and 7, when using the pseudo-inverse approach)—the plateau provided the highest correlation of approximately 0.70 for both the pseudo-inverse and post hoc filtering approaches, with higher tolerances/lower cutoff frequencies producing poorer correlation. For the pseudo-inverse approach, the stable stage consisted of all tolerance values below approximately 0.2–0.1. For the post hoc filtering approach, the plateau existed at cutoff frequencies above approximately

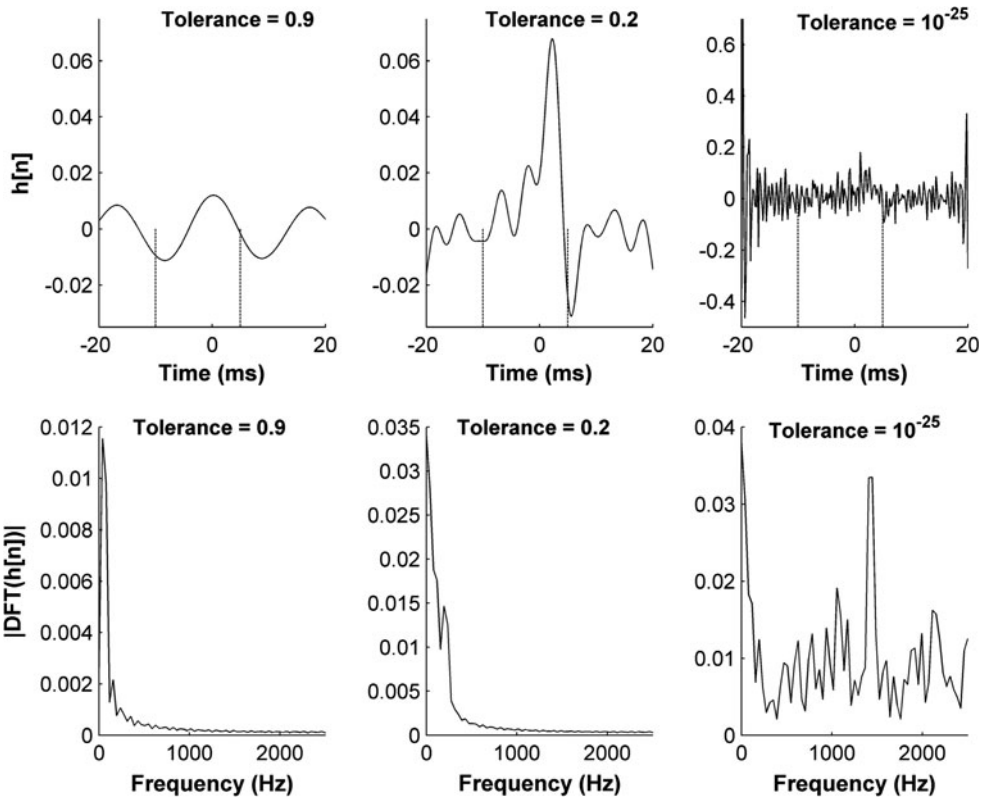

Fig. 3 Impulse responses (*top*) and their corresponding DFT magnitudes (*bottom*) using direct solution technique with pseudo-inverse tolerances as labeled. Subject GA01, $p_1 = 20$ ms, $p_2 = 20$ ms, $p_{1\_Extract} = 10$ ms and $p_{2\_Extract} = 5$ ms. *Dotted lines* in *top plots* indicate the $p_{1\_Extract}$ and $p_{2\_Extract}$ values. DFTs computed using impulse response from $p_{1\_Extract}$ to $p_{2\_Extract}$. Each plot uses distinct *y* axis

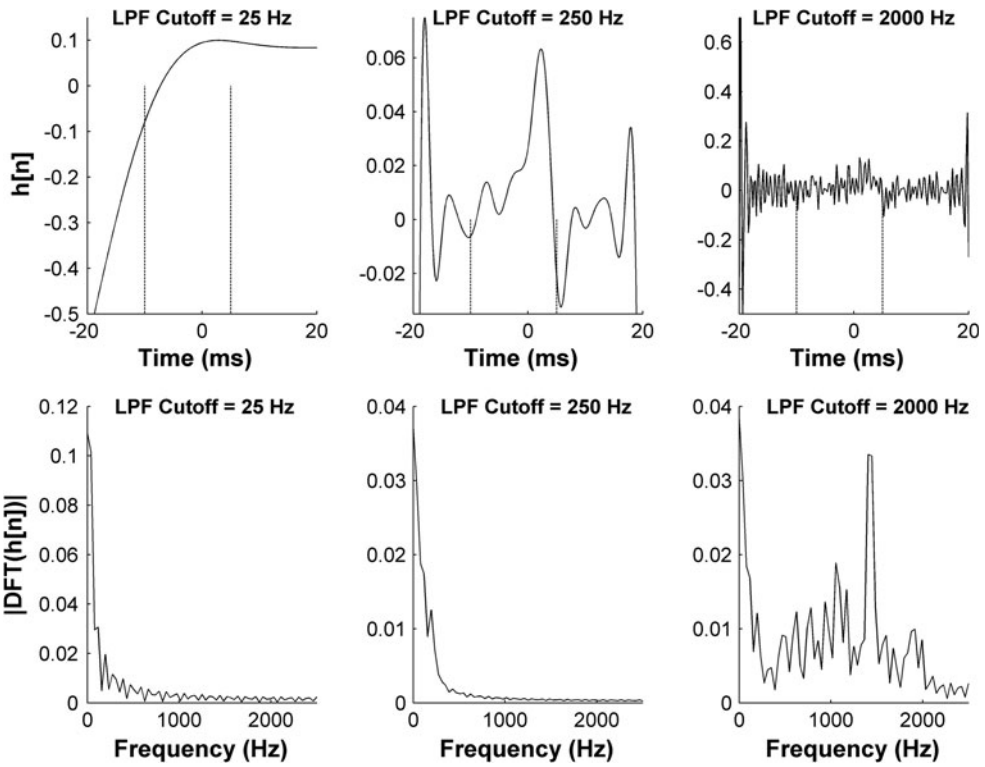

Fig. 4 Impulse responses (*top*) and their corresponding DFT magnitudes (*bottom*) using direct solution technique with post hoc low-pass filter cutoff frequencies as labeled. Subject GA01, $p_1 = 20$ ms, $p_2 = 20$ ms, $p_{1\_Extract} = 10$ ms and $p_{2\_Extract} = 5$ ms. *Dotted lines* in *top plots* indicate the $p_{1\_Extract}$ and $p_{2\_Extract}$ values. DFTs computed using impulse response from $p_{1\_Extract}$ to $p_{2\_Extract}$. Startup errors are visible outside of the $p_{1\_Extract}$ to $p_{2\_Extract}$ range. Each plot uses distinct y axis

250–300 Hz. Overall, the highest (i.e., best) cross-correlations were found using scenarios 5 and 6 (and 7, for the pseudo-inverse approach). Statistically, paired *t* tests compared results between each scenario pair for the pseudo-inverse approach at a tolerance of 0.1. All *p* values were Bonferroni adjusted. For the direct technique, scenarios 5–7

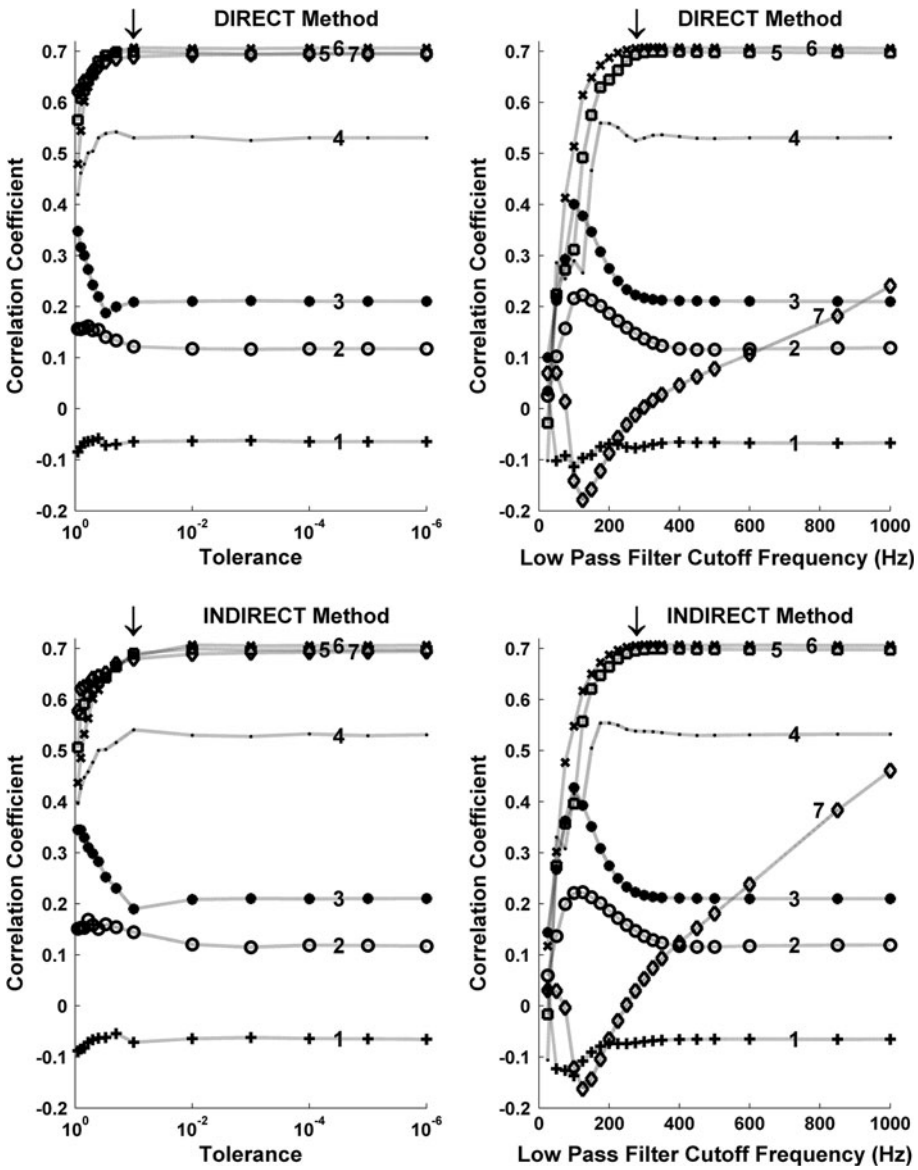

Fig. 5 Cross-correlation between model-predicted and measured "downstream" EMG signals versus pseudo-inverse tolerance(*left*) and low-pass filter cutoff frequency (*right*). *Top plots* use direct solution technique; *bottom plots* use indirect solution technique. Each result is the average of 72 test trials (36 subjects × 2 test trials/subject). Scenarios 1–7 denote results for distinct selections of p_1, p_2, $p_{1\_Extract}$ and $p_{2\_Extract}$, as enumerated in Table 1. *Arrows* indicate locations of optimal tolerance/ low-pass cutoff frequency

differed from each other scenario ($p < 0.0001$) and from each other ($p < 0.02$). For the indirect technique, scenarios 5–7 differed from each other scenario ($p < 0.0001$), but not from each other ($p > 0.13$). Similar paired *t* tests were performed for the low-pass filter approach, using results at 300 Hz. For both the direct and indirect techniques, scenarios 5–7 differed from each other scenario ($p < 0.0001$) and from each other ($p < 0.02$). In all cases when scenarios 5–7 showed statistical differences from each other, the difference in correlation values was quite small. An ANOVA compared the results of scenario 6 from each of the four pseudo-inverse/low-pass filter-direct/indirect combinations, using a tolerance of 0.1 and a filter cutoff of 300 Hz. These locations represent the best results, one per each of the four graphs in Fig. 5. The results were not significantly different [$F(3, 140) = 0.18$, $p = 0.91$)].

The last quantitative evaluation was between the "gold standard" mean conduction delay estimated via cross-correlation and that found by locating the peak of the impulse response. Figure 6 shows the average absolute differences between these methods. The optimal pseudo-inverse tolerance is approximately 0.5–0.2, with performance rapidly deteriorating for tolerances above 0.6. The optimal post hoc low-pass cutoff frequency occurs at approximately 200–250 Hz, with performance rapidly deteriorating at cutoff frequencies below 150 Hz. At these optimal locations, scenario 7 performed much poorer than all other scenarios. These optimal tolerance values/cutoff frequencies are adjacent to, but not overlapping with, those found for the correlation coefficient evaluations. In all cases, the optimal parameters provide an average delay difference of approximately 0.02 ms. Note that for typical conduction

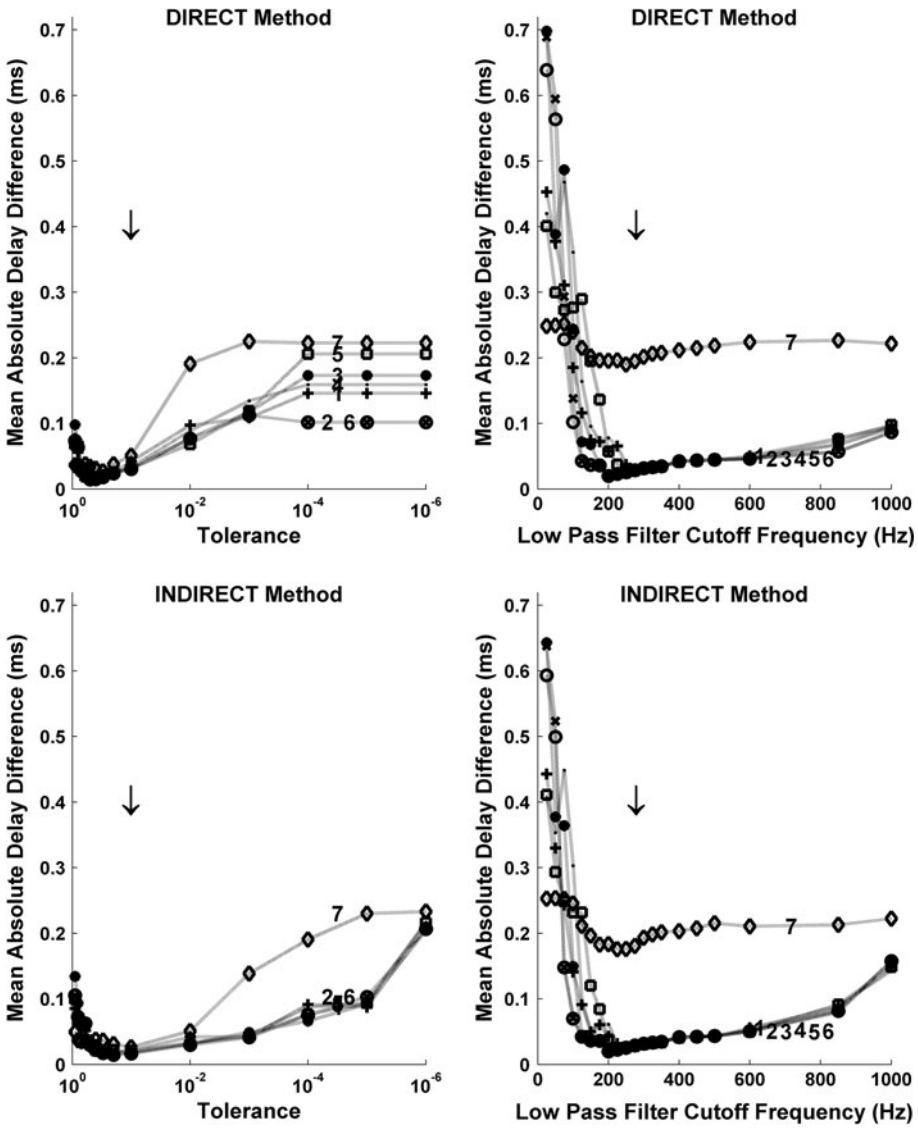

Fig. 6 Delay absolute difference between cross-correlation approach and the peak of the impulse response obtained from direct model (*top*) and indirect model (*bottom*) versus pseudo-inverse tolerance (*left*) and low-pass filter cutoff frequency (*right*). Each result is the average of 72 test trials (36 subjects × 2 test trials/subject). Scenarios 1–7 denote results for distinct selections of p_1, p_2, $p_{1\_Extract}$ and $p_{2\_Extract}$, as enumerated in Table 1. *Arrows* indicate locations of optimal tolerance/low-pass cutoff frequency

velocities between 3 and 5 m/s, electrodes placed at 10 mm spacing correspond to delays of 2–3.33 ms. Hence, errors at the best tolerance/cutoff are small. Statistically, paired *t* tests compared results between each scenario pair for the pseudo-inverse approach at a tolerance of 0.2. All *p* values were Bonferroni adjusted. For the direct technique, there were no differences ($p > 0.44$). For the indirect technique, there were no differences ($p > 0.15$) except comparing scenario 7 to all but scenario 5 ($p < 0.04$). Similar paired *t* tests were performed for the low-pass filter approach, using results at 200 Hz. For the direct technique, there were differences comparing scenario 1 to scenarios 2, 3, 6 and 7 ($p < 0.024$); and scenario 7 to all others ($p < 0.05$). For the indirect technique, there were differences when comparing to scenario 7 ($p < 0.032$). Except when considering scenario 7, when statistical differences were found, the differences in delay values were quite small. An ANOVA compared the results of scenario 6 from each of the four pseudo-inverse/low-pass filter-direct/indirect combinations, using a tolerance of 0.2 and filter cutoff of 200 Hz. These locations represent the best results, one per each of the four graphs in Fig. 6. The results were not significantly different [$F(3, 140) = 0.29$, $p = 0.83$)].

Lastly, a sample conduction delay probability density function (PDF) was estimated from the impulse response shown in the top middle plot of Fig. 3. The absolute value of the impulse response was taken, and its range restricted between 0 and 10 ms. The resulting plot was normalized to an area of one (Fig. 7, top left), as required by a PDF. The peak of this PDF indicates the mean conduction delay. However, the prevalence of large probabilities near zero time delay is not physiologic. Each discrete conduction delay along the time axis of this PDF maps to the relative conduction speed PDF via the equation: "speed = distance/delay",

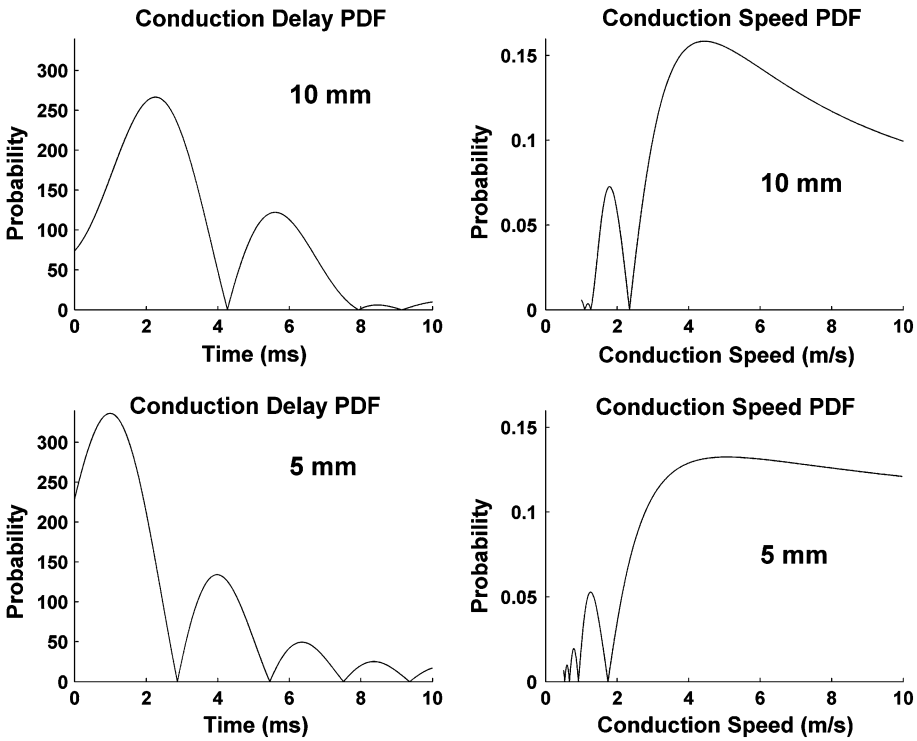

Fig. 7 *Top* estimated conduction delay probability density function (PDF) (*left*) and conduction speed PDF (*right*) for data corresponding to *top middle plot* of Fig. 3, 10-mm inter-electrode spacing. The impulse response used to form these estimates used the direct solution technique with pseudo-inverse tolerance value 0.2. Subject GA01, $p_1 = 20$ ms, $p_2 = 20$ ms, $p_{1\_Extract} = 10$ ms and $p_{2\_Extract} = 5$ ms. The conduction delay PDF is formed from the impulse response over the time range from 0 to 10 ms. Conduction speed PDF is formed from the conduction delay PDF. *Bottom* corresponding plots with 5 mm inter-electrode spacing

where "distance" is the inter-electrode distance of 10 mm and "delay" is the time delay (s). Each conduction delay value was mapped to its corresponding conduction speed, the speed axis was limited between 0 and 10 m/s and the resulting density area normalized to one (Fig. 7, top right). The prevalence of large probabilities at unrealistically high speeds (top right plot) is due to the high probability of low conduction delays (top left plot).

4 Discussion

This work investigated signal processing methods for estimating the impulse response between upstream and downstream EMG recordings. We found that the pseudo-inverse and post hoc low-pass filtering approaches both smooth the impulse response estimate in a nearly identical fashion. Too little smoothing produces impulse responses with erratic high-frequency content; too much smoothing obscures shape discrimination. Quantitative evaluation of model performance (Fig. 5) and comparison to "gold standard" estimates of *mean* conduction delay (Fig. 6) argue that, for these data, a pseudo-inverse tolerance value of $\sim$0.2 or a post hoc low-pass filter cutoff frequency of $\sim$250 Hz is optimal and produces strong results for these measures. As discussed further below, however, the impulse responses incorrectly contained substantive power at very low time delays.

Cross-correlation performance was quite sensitive to the time duration used to estimate the impulse response. For example, scenarios 2 and 6 differ only via parameter $p_{1\_Extract}$, which varies by only 1 ms. Yet, Fig. 5 shows substantial differences ($\sim$0.6) in their actual-to-estimated correlation. On the contrary, mean delay difference performance was quite similar for all scenarios (Fig. 6) except for scenario 7, which performed much poorer. This scenario is the only one that excludes "system anticipation", supporting the conclusion that it is needed to capture system dynamics [16]. The best performance across the three metrics was achieved by scenarios 5 and 6, which utilize very different signal ranges. Further, systematic, investigation into these sensitivities is appropriate.

The solution method of Hunter et al. [17] is reproduced herein as our indirect method, with either the smallest pseudo-inverse tolerance or highest low-pass filter cutoff (our scenario 7 should be excluded from comparison, since it does not include system anticipation). Figure 5 shows that the method of Hunter et al. provides an average cross-correlation that is indistinguishable from that of the best regularized estimate. However, Fig. 6 shows that the method of Hunter et al. is improved by our regularization approaches when considering average delay error. The mean absolute delay difference using the technique of Hunter et al. is 0.1–0.2 ms, compared to the best regularized value of 0.02 ms. The regularized methods can tune the degree of smoothing applied to the impulse response estimate.

While these regularization methods clearly improved the match between the impulse response-based *mean*

conduction delay and that found via traditional cross-correlation, the top middle panel of Figs. 3, and 7 shows a serious limitation in producing conduction delay *distribution* estimates from these data—our impulse function estimates incorrectly included substantial signal power at very low and at negative times, leading to high probabilities of overly short conduction delays. Unrealistic distribution estimates resulted. The dominant peak of the impulse response in Fig. 3 has a width of $\sim$4 ms, centered at $\sim$2 ms. The system identification requires an adequate amount of smoothing, else the peak is difficult to reliably distinguish—but smoothing spreads the peak. This constraint may be a fundamental limitation imposed by using such a small inter-electrode distance (10 mm). To assess this hypothesis, recall that our experimental protocol also collected upstream and downstream EMG with 5 mm inter-electrode spacing. The bottom plots in Fig. 7 show the delay and speed PDF estimates from the same trial, using the corresponding 5-mm inter-electrode data. The 5-mm data demonstrate a larger proportion of conduction delay probabilities near zero delay. Therefore, the most appropriate solution may be to use a larger inter-electrode spacing. At a conduction velocity of 3–5 m/s, each additional inter-electrode spacing of 5 mm delays the impulse response peak by 1–1.67 ms. Hence, a minimum inter-electrode spacing of 15–20 mm may be required to delay the main peak away from zero time, facilitating delay *distribution* estimation.

While this method of impulse response estimation relies on simple recordings from two conventional bipolar electrodes, the underlying analytic model of Williams [30] assumes that the EMG due to individual MUs sum to produce the interference pattern, that the action potential shape of each MU is identical and that each MU action potential arrives at the "downstream" electrode site after a pure delay. In reality, the action potentials of distinct MUs vary in shape. Hence, our delay distribution is weighted more heavily by larger amplitude MUs. The physical alignment of muscle fibers is not perfectly straight, inferring that the action potential shape recorded from the upstream electrode is not identical to that recorded downstream. Bipolar recordings can include substantial common-mode components which skew the delay distribution towards a physiologically impossible delay of zero time. In our application, common-mode components could have contributed to the substantial impulse response power near zero time delay. This issue might be minimized by double-difference electrodes [3, 12, 23, 27]. In addition, although our signal model (see Fig. 1) includes noise in both recorded signals, our impulse response estimation methods do not explicitly describe the influence of these noises. For example, Eq. 2 shows that the input noise is propagated to the output via convolution with the impulse response. Alternative system identification techniques might be more effective in attenuating the influence of these specific noise sources based on their statistical characterizations.

Another result of the Williams [30] model and its assumptions is that the impulse response is expected to exist only over times that correspond to viable delays and be non-negative in value at all times. In practice, we have already noted the problem of impulse response signal power near zero time and at negative times. In our delay distribution estimates (Fig. 7), we ignored such out-of-range times. But doing so clearly violates the model assumptions. Further, Figs. 3 and 4 show substantive time durations during which the impulse response values are negative. Such values present a model conflict. We followed the approach of Hunter et al. [17] by taking the absolute value of the impulse response function when producing the delay distribution. But, these adjustments may have significantly distorted the delay distribution estimates. It seems reasonable to first resolve the issue of too much impulse response signal power near/before zero time, which might also impact the prevalence of negative-valued time regions. Thereafter, an approach to resolve negative-valued impulse response values might be to parameterize the impulse response time-series itself via non-negative functions (e.g., Gaussian functions truncated in time). A different parameter estimation problem would result, likely with other strengths and weaknesses.

A number of the above issues might be examined in the future with simulation models, based on the interference signal model shown in Fig. 1 and/or the underlying physiology of motor units (e.g., [30]). With simulation models, the "true" system is known, permitting direct measures of performance. Another advantage of such models is that individual issues that might confound delay distribution estimation—e.g., common-mode signals, recording noise, electrode spacing/alignment, system identification methods—can be individually and precisely controlled. Additionally, the role of certain assumptions of the models could be studied.

Westwick and Kearney [29] applied a singular-value-decomposition-based pseudo-inverse approach to solve for the impulse response based on the model and "indirect" solution of Hunter et al. [17]. Their approach evaluated a single pseudo-inverse tolerance cutoff, but adapted that cutoff to the noise characteristics of each individual trial (greater than 95 % probability that retained singular values represented signal rather than noise). This approach explicitly trades off random/variance error (found when retaining too many singular values) versus bias error (generated as singular values are discarded from the inverse). The technique also produces trial-by-trial confidence bounds on the impulse response estimates. They tested their method in simulation (model shown in Fig. 1

with the input noise omitted) and in an example application estimating joint dynamics about the ankle. They also evaluated post hoc smoothing of the unregularized impulse response, testing a single cutoff frequency. Their simulation results clearly demonstrate the phenomenon of high-frequency noise in the unregularized impulse response estimate, as we have found using our EMG data. Similarly, they also found a high degree of agreement between the actual and model-estimated output signal, regardless of the impulse response estimation method. Their approach provided far better estimates of the known "true" impulse response function as compared to the method of Hunter et al. and somewhat better performance (2–3 %) than their post hoc smoother. Their method of estimating the impulse response is attractive, since it directly accounts for noise by adjusting the pseudo-inverse tolerance to the noise characteristics of each trial, which can vary. A disadvantage is that the noise characteristics of a signal are not always well estimated from a single recording. In the future, it might be useful to apply their method to the EMG delay problem and study the influence of the pseudo-inverse tolerance selection. Is performance improved by varying the tolerance cutoff based on the noise statistics of each trial, or is a more stable cutoff selection (averaged across the subject population, as in our investigation) more advantageous? Note that trial-by-trial methods for selection of an appropriate post hoc low-pass filter selection might similarly be considered. The coherence function between the upstream and downstream EMG could be used as a guide [17].

In summary, we analyzed the surface EMG from pairs of bipolar electrodes placed on the tibialis anterior of 36 subjects, using an inter-electrode distance of 10 mm. We modeled the impulse response between the electrodes with a FIR structure using direct and indirect model-fitting methods and two techniques to regularize the least squares fit (pseudo-inverse and post hoc low-pass filtering). Both regularization methods smoothed the impulse response in a similar manner. Inadequate smoothing led to high-frequency interference while excessive smoothing impeded shape discrimination. Optimal smoothing occurred with a pseudo-inverse tolerance of ~ 0.2 or a post hoc low-pass filter cutoff frequency of ~ 250 Hz. The resulting impulse response was evaluated by correlating the actual downstream EMG with that found by filtering the upstream EMG through the impulse response model, giving an average correlation coefficient of 0.70. Additionally, *mean* conduction delay, taken as the time of the peak impulse response, was compared to the traditional approach of cross-correlating the upstream and downstream EMG signals. The average error was 0.02 ms. These results show excellent model performance. Nonetheless, the resulting impulse responses incorrectly included substantive power at very low and negative time delays, causing delay *distribution* estimates to exhibit high probabilities at very short conduction delays. Unrealistic distribution estimates resulted. Thus, none of the impulse response estimation methods studied can be considered successful for use in forming delay distribution estimates with these data. Larger inter-electrode spacing (15–20 mm) may be required to alleviate this fundamental limitation.

References

1. Blijham PJ, Hengstman GJD, Ter Laak HJ, Van Engelen BGM, Zwarts MJ (2004) Muscle-fiber conduction velocity and electromyography as diagnostic tools in patients with suspected inflammatory myopathy: a prospective study. Muscle Nerve 29:46–50
2. Blijham PJ, Ter Laak HJ, Schelhaas HJ, Van Engelen BGM, Stegeman DF, Zwarts MJ (2006) Relation between muscle fiber conduction velocity and fiber size in neuromuscular disorders. J Appl Physiol 100:1837–1841
3. Broman H, Bilotto G, DeLuca CJ (1985) A note on the noninvasive estimation of muscle fiber conduction velocity. IEEE Trans Biomed Eng 32:341–344
4. Chaffin DB (1973) Localized muscle fatigue—definition and measurement. J Occup Environ Med 15:346–354
5. Davies SW, Parker PA (1987) Estimation of myoelectric conduction velocity distribution. IEEE Trans Biomed Eng 34:365–374
6. Farina D, Merletti R (2003) A novel approach for estimating muscle fiber conduction velocity by spatial and temporal filtering of surface EMG signals. IEEE Trans Biomed Eng 50:1340–1351
7. Farina D, Merletti R (2004) Methods for estimating muscle fibre conduction velocity from surface electromyographic signals. Med Biol Eng Comput 42:432–445
8. Farina D, Mesin L (2005) Sensitivity of surface EMG-based conduction velocity estimates to local tissue in-homogeneities—influence of the number of channels and inter-channel distance. J Neurosci Meth 142:83–89
9. Farina D, Negro F (2007) Estimation of muscle fiber conduction velocity with a spectral multidip approach. IEEE Trans Biomed Eng 54:1583–1589
10. Farina D, Fortunato E, Merletti R (2000) Noninvasive estimation of motor unit conduction velocity distribution using linear electrode arrays. IEEE Trans Biomed Eng 47:380–388
11. Farina D, Muhammad W, Fortunato E, Meste O, Merletti R, Rix H (2001) Estimation of single motor unit conduction velocity from surface electromyogram signals detected with linear electrode arrays. Med Biol Eng Comput 39:225–236
12. Farina D, Arendt-Nielsen L, Merletti R, Graven-Nielsen T (2002) Assessment of single motor unit conduction velocity during sustained contractions of the tibialis anterior muscle with advanced spike triggered averaging. J Neurosci Meth 115:1–12
13. Farina D, Zagari D, Gazzoni M, Merletti R (2004) Reproducibility of muscle-fiber conduction velocity estimates using multichannel surface EMG techniques. Muscle Nerve 29:282–291
14. Gazzoni M, Farina D, Merletti R (2004) A new method for the extraction and classification of single motor unit action potentials from surface EMG signals. J Neurosci Meth 136:165–177
15. Gydikov A (1981) Spreading of potentials along the muscle, investigated by averaging of the summated EMG. Electromyogr Clin Neurophysiol 21:525–538
16. Hunter I, Kearney R (1983) Two-sided linear filter identification. Med Biol Eng Comput 21:203–209

17. Hunter I, Kearney R, Jones L (1987) Estimation of the conduction velocity of muscle action potentials using phase and impulse response function techniques. Med Biol Eng Comput 25:121–126
18. Lindstrom LH, Magnusson RI (1977) Interpretation of myoelectric power spectra: a model and its applications. Proc IEEE 65:653–662
19. Lynn PA (1979) Direct on-line estimation of muscle fiber conduction velocity by surface electromyography. IEEE Trans Biomed Eng 26:564–571
20. Masuda T, Miyano H, Sadoyama T (1982) The measurement of muscle fiber conduction velocity using a gradient threshold zero-crossing method. IEEE Trans Biomed Eng 29:673–678
21. McIntosh KCD (2009) Reliability of muscle fibres conduction velocity in the tibialis anterior. M.S. thesis, Brock University, Ontario, Canada
22. McIntosh K, Gabriel D (2012) Reliability of a simple method for determining muscle fiber conduction velocity. Muscle Nerve 45:257–265
23. Mesin L, Tizzani F, Farina D (2006) Estimation of motor unit conduction velocity from surface EMG recordings by signal-based selection of the spatial filters. IEEE Trans Biomed Eng 53:1963–1971
24. Naeije M, Zorn H (1982) Relation between EMG power spectrum shifts and muscle fibre action potential conduction velocity changes during local muscular fatigue in man. Eur J Appl Physiol 50:23–33
25. Press WH, Teukolsky SA, Vetterling WT, Flannery BP (1994) Numerical recipes in C, 2nd edn. Cambridge University Press, New York, pp 671–681
26. Rababy N, Kearney R, Hunter I (1989) Method for EMG conduction velocity estimation which accounts for input and output noise. Med Biol Eng Comput 27:125–129
27. Schulte E, Farina D, Rau G, Merletti R, Disselhorst-Klug C (2003) Single motor unit analysis from spatially filtered surface electromyogram signals. Part 2: conduction velocity estimation. Med Biol Eng Comput 41:338–345
28. Viitasalo JHT, Komi PV (1977) Signal characteristics of EMG during fatigue. Eur J Appl Physiol 37:111–121
29. Westwick DT, Kearney RE (1997) Identification of physiological systems: a robust method for non-parametric impulse response estimation. Med Biol Eng Comput 35:83–90
30. Williams WJ (1972) Transfer characteristics of dispersive nerve bundles. IEEE Trans Sys Man Cyber 2:72–85
31. Zwarts MJ, Stegeman DF (2003) Multichannel surface EMG: basic aspects and clinical utility. Muscle Nerve 28:1–17
32. Zwarts MJ, Van Weerden TW, Haenen HTM (1987) Relationship between average muscle fibre conduction velocity and EMG power spectra during isometric contraction, recovery and applied ischemia. Eur J Appl Physiol 56:212–216
33. Zwarts MJ, Drost G, Stegeman DF (2000) Recent progress in the diagnostic use of surface EMG for neurological diseases. J Electromyogr Kinesiol 10:287–291